USING MATHEMATICAL ABSORBER REFLECTION SUPPRESSION (MARS) TO PARTIALLY CORRECT FOR THE NON-UNIFORMITY OF A CATR QUIET ZONE

S.F. Gregson[(1)], C.G. Parini[(2)], A.C. Newell[(3)], P.N. Betjes[(4)]

[(1)] NSI-MI, 19730 Magellan Drive, Torrance, CA 90502, USA, sgregson@nsi-mi.com
[(2)] Queen Mary University of London, 10 Godward Square London E1 4FZ, UK, c.g.parini@qmul.ac.uk
[(3)] NSI-MI, 19730 Magellan Drive, Torrance, CA 90502, USA, anewell@nsi-mi.com
[(4)] NSI-MI, 19730 Magellan Drive, Torrance, CA 90502, USA, pbetjes@nsi-mi.com

***Abstract* – This paper extends a previous study in which a new computational electromagnetic (CEM) modelling tool was developed that allowed prediction of "measured" far-field antenna pattern data, including range related errors, for a known compact antenna test range (CATR) and antenna under test (AUT) combination [1, 2, 3, 4, 5] to be computed. This paper extends that work and, for the first time, shows how the deleterious effects of amplitude ripple and phase ripple within the CATR pseudo plane wave can be largely mitigated using the far-field implementation of the measurement and post-processing technique called mathematical absorber reflection suppression (MARS) [4, 6]. Hitherto, the various implementations of MARS have been used to identify and subsequently suppress various errors within all forms of near-field and far-field antenna measurements such as range reflections truncation *etc.* [4], however this is the first time that MARS has been used to improve the quality of measurements made using a given CATR by improving the uniformity of the pseudo plane wave. Results are presented and discussed.**

I. INTRODUCTION

The point source compact antenna test range (CATR) uses a parabolic reflector to project an image of the feed antenna to infinity which has the effect of transforming the quasi-spherical wave that is radiated by the feed antenna (which is positioned at the focal point of the reflector) into a pseudo plane wave which is used to illuminate the antenna under test (AUT) thereby synthesising the classical far-field measurement configuration only, at a greatly reduced physical distance. The widely accepted criteria for specifying the quality of this pseudo plane is to insure that the wave should have less than a 1 dB amplitude taper, less than a ±0.5 dB amplitude ripple and less than a ±5° phase ripple [1]. The amplitude taper is measured as the variation of a quadratic function that is typically found from a least squares best fit through the amplitude data over a cut through the quiet zone (QZ). The amplitude ripple is then measured by determining the variation of the amplitude about this 2nd degree polynomial function. The phase ripple is characterized by the deviation from a best-fit straight line across the QZ and is expressed in decimal degrees. These linear cuts are typically acquired across horizontal, vertical or inter-cardinal cuts that are transverse to the *z*-axis of the range and are repeated for various z positions down range. The maximum dimensions within a volume of space, typically cylindrical in shape, throughout which this specification can be met determines the physical size of the CATR QZ [1]. Amplitude taper and amplitude ripple parameters are illustrated in Figure 1 with the phase ripple being analogous to the amplitude pattern without the quadratic taper. These field properties are generally measured as part of the CATR installation using a procedure based upon a field probe scanner [1, 3]. The final facility acceptance is typically predicated upon the vendor being able to successfully demonstrate that these requirements have been met or exceeded at a number of specified frequencies.

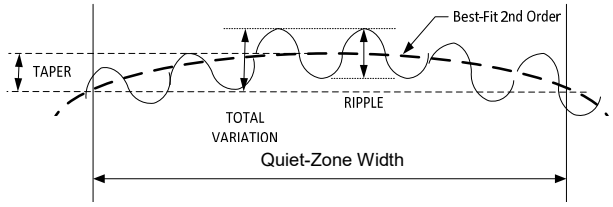

Figure 1: Illustration of CATR amplitude taper and amplitude ripple specifications in the QZ.

II. OVERVIEW OF CATR MODELLING

As noted above and as developed in [1], the coupling of the pseudo plane-wave into the aperture of an AUT creates the classical measured "far-field" radiation pattern. Assuming the electric and magnetic fields radiated by a given antenna over the convenient enclosing surface are known then, it is possible to create a perfect plane wave and to use that to sample the far-field antenna pattern in a specific far-field direction by evaluating the reaction integral between the plane wave and the AUT. The electric and magnetic fields of a perfect *x*-polarised plane wave propagating in the positive *z*-direction can be expressed as,

$$\underline{E}(x,y,z) = A(x,y)e^{-jk_0 z}\,\underline{\hat{e}}_x \qquad (1)$$

Here we have assumed a positive, supressed, time

dependency, A is the complex wave amplitude and k_0 is the free-space propagation constant. Thus, we can create a plane wave with amplitude taper, amplitude ripple and phase ripple of our choosing using, for example,

$$A(x,y)=\sin\left(\frac{n_x\pi x}{L_x}\right)\sin\left(\frac{n_y\pi y}{L_y}\right) \quad (2)$$

Here, n_x, n_y denotes the number of ripples in the x- and y-axes respectively and L_x, L_y denote the width of the CATR QZ in the x- and y-axes. Similar expressions can be used to perturb the phase function. The corresponding magnetic fields can be obtained from the TEM condition as the direction of propagation is the z-axis and,

$$\underline{H}(x,y,z)=\frac{1}{Z_0}\hat{\underline{u}}\times\underline{E}(x,y,z) \quad (3)$$

Here, Z_0 is the characteristic impedance of free space. The "measured" far-field patterns for a given CATR AUT combination can be obtained from an application of the reaction theorem which is a well-known method for analysing coupling problems [1]. This theorem states that, provided the electric *and* magnetic field vectors ($\underline{E}_1$, $\underline{H}_1$) and ($\underline{E}_2$, $\underline{H}_2$) are of the same frequency and monochromatic then the mutual impedance, Z_{21}, between two radiators, antenna 1 (*i.e.* the CATR) and antenna 2 (*i.e.* the AUT), in the homogeneous and isotropic environment described by ε, μ can be stated in terms of a closed surface integration.

$$Z_{21}=\frac{V_{21}}{I_{11}}=-\frac{1}{I_{11}I_{22}}\int_{S_2}\left(\underline{E}_2\times\underline{H}_1-\underline{E}_1\times\underline{H}_2\right)\cdot\hat{\underline{n}}\,ds \quad (4)$$

The mutual impedance will clearly be a function of the displacement between the two antennas, their respective orientations, and their relative polarisation properties. Once the mutual impedance, and therefore the mutual admittance is known, it is a comparatively straight forward task to obtain the transmission scattering parameter S_{21} that related the two coupled two-port scattering matrices [1]. The elements $S_{12} = S_{21}$ are the complex transmission coefficients for the coupled antenna system which can be taken to represent a single point within the "measured" far-field pattern. This integration can, in principle, be performed over any convenient free-space closed surface however a great deal of computational efficiency and simplicity can be sought if a spherical integrating surface is chosen. Although in principal any closed surface could be used, the advantage of adopting a spherical surface is that a general compound rotation can be implemented without the need to compute fields *outside* of this sampling interval. Such vector isometric rotations can be implemented either approximately [4] or rigorously, by expanding the fields onto a set of spherical vector mode functions and by rotating those mode coefficients [7]. When utilising this reaction based technique to simulate CATR measurements it is crucial to notice that the fields illuminating the AUT from the CATR need to be computed only *once* per frequency. This is also the case for the fields radiated by the AUT which makes the processing very efficient [1, 3].

III. Overview of Far-field MARS

For conventional CATR measurements it is customary for the AUT to be carefully installed within the facility such that the AUT is situated about the axis of rotation, *i.e.* at the origin of the measurement coordinate system. This has the effect of minimizing the volume of the QZ needed and limiting the difference between the direct and indirect (*i.e.* scattered) illumination. However, when taking a "MARS" type measurement, and contrary to usual practice, the AUT is deliberately displaced from the centre of rotation. This has the effect of making the differences between the illuminating field and any scattered field appear to be far more pronounced than would otherwise be the case which makes their identification and subsequent extraction viable. In summary, the far-field MARS algorithm can be described as follows [4, 6, 8] and is predicated on standard cylindrical near-field theory [4]:

1. Take a direct acquisition of the one-dimensional far field amplitude and phase pattern with the AUT offset from the measurement origin.
2. Apply a phase change to mathematically translate the AUT back to the origin of the measurement coordinate system.
3. Obtain the translated cylindrical mode coefficients (CMCs) of the AUT for an AUT conceptually located at the origin of the measurement coordinate system.
4. Apply band pass filtering function to suppress unwanted higher order modes where the properties of the filter function are determined from the physical size of the AUT and the frequency.
5. Re-compute the far field pattern from the filtered mode coefficients to obtain the FF-MARS filtered AUT pattern.

It has been well established that far-field MARS processing is a highly effective technique for supressing range reflections and feed spill-over in CATRS [4, 6, 8, 9]. However, for the first time, this paper presents the results of a study that examines the effectiveness of FF-MARS in improving the performance of an existing CATR by digitally compensating for imperfections within the uniformity of the pseudo plane wave. The results of this study are presented in the following section.

IV. Preliminary Results

In order that the effectiveness of the FF-MARS technique could be verified a number of simulations were run. In each case an x-band SG90 pyramidal horn was used as the AUT. This antenna was positioned offset from the origin of the measurement coordinate

system by 0.61 m. The electromagnetic six-vector was computed over the surface of a conceptual integrating sphere with a radius of 0.91 m with a data point spacing of 1° in the θ and ϕ at a frequency of 8 GHz. The CATR pseudo TEM wave was then fashioned by using equations (1) through (3) with the amplitude and phase ripple being varied for each case. As with the AUT, a spherical sampling surface of 0.91 m radius was used. Five test cases were initially considered. For these simulations all parameters were held consistent with the exception of the spatial frequency of the amplitude and phase ripple across the pseudo plane wave, which was varied from 10 ripples to 50 ripples in steps of 10. The amplitude taper of the pseudo plane wave was set to 0 dB (*i.e.* no amplitude taper) as this is not a property that FF-MARS is able to mitigate. Figures 2, 4, 6, 8 and 10 present the great circle azimuth amplitude cut of the "measured" AUT pattern for the cases where the pseudo plane wave had 50, 40, 30, 20 and 10 ripples respectively across the 1.8 m CATR QZ. The peak to peak amplitude ripple was 1 dB and the peak-to-peak phase ripple was 10°. The blue trace denotes the ideal far-field pattern of the pyramidal horn which we take as the reference amplitude pattern. The red trace represents the "measured" far-field pattern, *i.e.* the far-field pattern that would be obtained with using the perturbed CATR pseudo-plane wave, the black trace denotes the FF-MARS processed pattern and the difference between the reference and FF-MARS processed patterns is shown with the magenta trace. This corresponds to the local linear difference between the two patterns when expressed in dB form. Thus, the better the agreement the larger the negative value until when the two patterns are in perfect agreement the dB difference level would be -∞ dB. The root mean square (RMS) of this difference level is also computed for each case and is shown in the respective plots and summarised in Table 1 below. Similarly, Figures 3, 5, 7, 9 and 11 present the far-field great circle phase plots for the 50, 40, 30, 20 and 10 ripples respectively across the 1.8 m CATR QZ. Here, a consistent colour scheme was adopted with the reference phase pattern being plotted in blue, the perturbed far-field phase pattern is shown in red and the FF-MARS processed phase plot is shown in black.

Table 1: Summary of results showing improvement provided by FF-MARS processing as CATR QZ ripple spatial frequency changes.

No. of ripples across QZ	RMS diff without (dB)	RMS diff with (dB)	FF-MARS Change (dB)
50	-42.8	-62.7	19.9
40	-42.8	-62.5	19.7
30	-41.3	-61.9	20.5
20	-40.8	-49.7	8.9
10	-39.8	-41.7	1.9

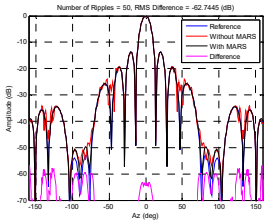

Figure 2: FF Amplitude plot for 50 ripples across QZ.

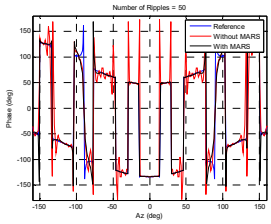

Figure 3: FF Phase plot for 50 ripples across QZ.

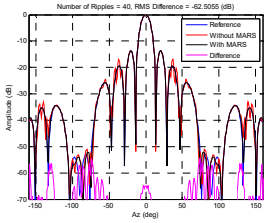

Figure 4: FF Amplitude plot for 40 ripples across QZ.

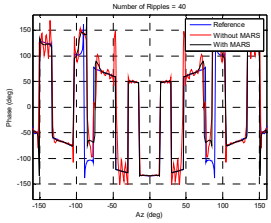

Figure 5: FF Phase plot for 40 ripples across QZ.

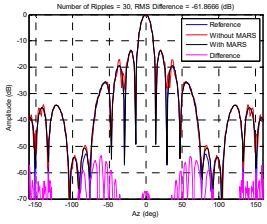

Figure 6: FF Amplitude plot for 30 ripples across QZ.

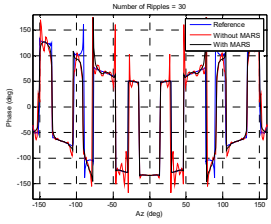

Figure 7: FF Phase plot for 30 ripples across QZ.

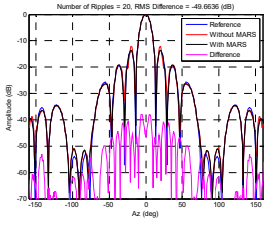

Figure 8: FF Amplitude plot for 20 ripples across QZ.

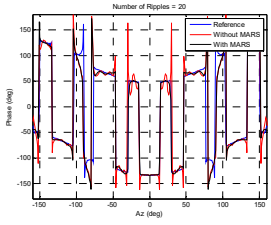

Figure 9: FF Phase plot for 20 ripples across QZ.

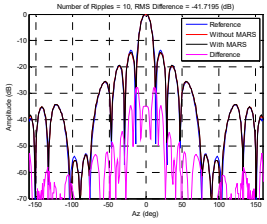

Figure 10: FF Amplitude plot for 10 ripples across QZ.

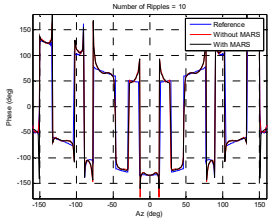

Figure 11: FF Phase plot for 10 ripples across QZ.

From inspection of these plots is it evident that FF-MARS processing is very effectively compensating for the errors in the far-field pattern that are introduced by the ripple in pseudo plane wave for cases where the spatial frequency is higher. Table 1 above summarises these results and from inspection of the results shown it is clear that for the cases where the spatial frequency is *circa* 30 ripples across the 1.8 m CATR QZ or more, then the measurement errors are very effectively being identified and extracted with a circa 20 dB improvement in the RMS difference level being achieved.

Conceptually, amplitude and phase ripple across the pseudo plane wave can be considered to result from the interference of two, or more, plane wave propagating in different directions interfering constructively and destructively across the plane. The larger the angle between the directions of propagation of these waves the higher the spatial frequency of the ripple in resulting interference pattern. When the direction of arrival of these plane waves is close to that of the ideal pseudo plane wave then it is going to be very difficult for the MARS processing to extract the undesired wave. However, when the direction of arrival is larger, and the spatial frequency of the interference pattern is higher, this wave can be far more easily differentiated from the ideal pseudo plane wave when viewed in the mode domain.

In order that this could be more easily examined, the cylindrical mode coefficient (CMCs) plots can be seen presented in Figures 12, 13, 14, 15, and 16 which correspond to the 50, 40, 20, 20 and 10 ripple cases respectively. Here, the red trace represents the CMCs that are computed from the far-field pattern data once the AUT has been translated back to the origin of the measurement coordinate system. The blue trace represents those CMCs that, by virtue of the cylindrical sampling theorem, correspond to the AUT alone.

Here, cylindrical mode coefficients (CMC) are complex numbers that are functions of frequency, the polarization index, and the azimuthal index which do not vary with any of the scanning coordinates [4]. The cylindrical mode cut-off is determined by evaluating when $|n| \leq \text{ceil}(k_0 r_{t0}) + n_s$ where n is the highest order cylindrical mode index associated with the AUT. Here, r_{t0} denotes the maximum radial extent (MRE) [4], k_0 is the free space propagation number, n_s is a positive integer that is used as a safety margin that depends upon the accuracy required and ceil is a function that rounds towards positive infinity. The MRE is the radius of a conceptual cylinder that is centered about the origin of the measurement coordinate system that is large enough to circumscribe the majority of the current sources in the AUT [3, 4, 6, 8, 9]. Thus, by knowing the physical size of the AUT, the frequency then it is possible to set the limit of the band-pass mode filter function. Here, a $\cos^2$ mode filter function is used so as to match as many derivatives of the windowing function to zero as possible as this is known to improve the phase results of the resulting FF-MARS processed far-field pattern [10].

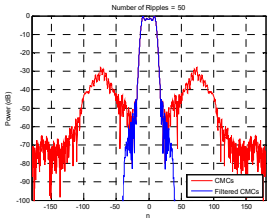

Figure 12: CMC plot for 50 ripples case.

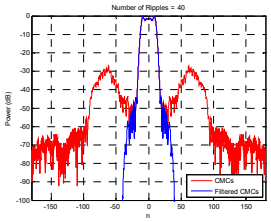

Figure 13: CMC plot for 40 ripples case.

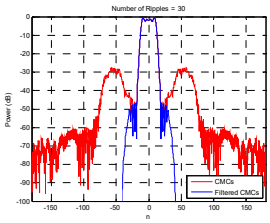

Figure 14: CMC plot for 30 ripples case.

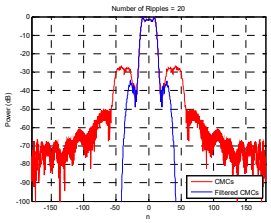

Figure 15 CMC plot for 20 ripples case.

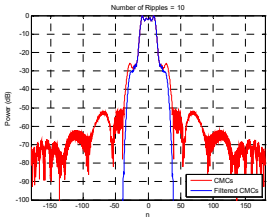

Figure 16 CMC plot for 10 ripples case.

From inspection of these figures, *i.e.* 12 - 16, it is clear that as the spatial frequency of the ripple on the CATR pseudo plane wave increases, so too does the amount of power present in the higher order modes of the cylindrical mode expansion, *cf.* Figure 12. Conversely, as the spatial frequency decreases those modes associated with the ripple gradually shift to lower order mode coefficients and increasingly coexist with those modes associated with the AUT rendering their extraction through mode filtering ineffectual, *cf.* Figure 16. However, as the spatial frequency of the ripple increases, corresponding conceptually to incoming waves at wider angles of incidence, the mode spectra shift towards higher order mode spectra whereupon they can be extracted with the application of a band-pass mode filter. Table 2 below presents a comparison of the improvement obtained using FF-MARS processing against the number of wavelengths (λ) per ripple. This table also shows the inverse quantity, *i.e.* the number of ripples per wavelength with the results being taken across the 48 wavelengths span of the 1.8 m CATR QZ for the 8.0 GHz test frequency. This suggests that providing we have more than half a ripple per wavelength then the FF-MARS processing appears to be effective. However, this is a very preliminary result and requires further verification to establish its generality.

Table 2: Summary of ripple rate and FF-MARS Improvement

No. of ripples across QZ	λ/Ripple	Ripples/λ	FF-MARS Improvement (dB)
50	0.96	1.0417	19.9
40	1.20	0.8333	19.7
30	1.60	0.6250	20.5
20	2.40	0.4167	8.9
10	4.80	0.2083	1.9

V. SUMMARY AND CONCLUSION

This paper summarises the findings of an on-going programme of research that for the first time has demonstrated that FF-MARS can be used to suppress the effects of imperfections within the uniformity of the pseudo plane wave. As this is an ongoing programme of work, and as the effectiveness of FF-MARS has been demonstrated in this area of application, the planned future work is to include extending the simulation to include more complex field distributions, *i.e.* spectral content, so as to be able better able to established the limits of applicability of the technique.

VI. REFERENCES

[1] C.G. Parini, R. Dubrovka, S.F. Gregson, "CATR Quiet Zone Modelling and the Prediction of "Measured" Radiation Pattern Errors: Comparison using a Variety of Electromagnetic Simulation Methods" AMTA October 2015.

[2] C.G. Parini, R. Dubrovka, S.F. Gregson, "Computational Electromagnetic Modelling of Compact Antenna Test Range Quiet Zone Probing: A Comparison of Simulation Techniques", EuCAP, Davos, Switzerland, April, 2016.

[3] S.F. Gregson, C.G. Parini, "Examination of the Effect of Common CATR Quiet Zone Specifications on Antenna Pattern Measurement Uncertainties", Loughborough Antennas and Propagation Conference, November 2017.

[4] C.G. Parini, S.F. Gregson, J. McCormick, D. Janse van Rensburg "Theory and Practice of Modern Antenna Range Measurements", IET Press, 2014, ISBN 978-1-84919-560-7.

[5] D. Hess; F. Willwerth; R. Johnson, "Compact range improvements and performance at 30 GHz", 1977 Antennas and Propagation Society International Symposium Year: 1977, Volume: 15 Pages: 264 - 267, DOI: 10.1109/APS.1977.1147853.

[6] S.F. Gregson, J. Dupuy, C.G. Parini, A.C. Newell, G.E. Hindman, "Application of Mathematical Absorber Reflection Suppression to Far-Field Antenna Measurements" Loughborough Antennas and Propagation Conference, 2011.

[7] J.E. Hansen, "Spherical Near-Field Antenna Measurements", IEE Electromagnetic Waves Series 26, ISBN 0 86341 110X, 1988.

[8] S.F. Gregson, B. Williams, G.F. Masters, A.C. Newell, G.E. Hindman, "Application of Mathematical Absorber Reflection Suppression To Direct Far-Field Antenna Range Measurements", AMTA, October, 2011.

[9] S.F. Gregson, A.C. Newell, C.G. Parini, "Verification of Feed Spill-over Reduction using FF-MARS in a CATR Using Computational Electromagnetic Simulation", IEEE Antennas and Propagation Society, Symposium, San Diego, July 2017.

[10] S.F. Gregson, C.G. Parini, A.C. Newell, G.E. Hindman, "Examination of the Effectiveness of Far-field Mathematical Absorber Reflection Suppression in a CATR Through Computational Electromagnetic Simulation", European Conference on Antennas and Propagation, Paris, March, 2017.